MATHEMATICS OF THE FARADAY CAGE

S. JONATHAN CHAPMAN*, DAVID P. HEWETT†, AND LLOYD N. TREFETHEN‡

Abstract. The amplitude of the gradient of a potential inside a wire cage is investigated, with particular attention to the 2D configuration of a ring of n disks of radius r held at equal potential. The Faraday shielding effect depends upon the wires having finite radius and is weaker than one might expect, scaling as $|\log r|/n$ in an appropriate regime of small r and large n. Both numerical results and a mathematical theorem are provided. By the method of multiple scales, a continuum approximation is then derived in the form of a homogenized boundary condition for the Laplace equation along a curve. The homogenized equation reveals that in a Faraday cage, charge moves so as to somewhat cancel an external field, but not enough for the cancellation to be fully effective. Physically, the effect is one of electrostatic induction in a surface of limited capacitance. An alternative discrete model of the effect is also derived based on a principle of energy minimization. Extensions to electromagnetic waves and 3D geometries are mentioned.

Key words. Faraday cage, shielding, screening, homogenization, harmonic function

AMS subject classifications. 31A35, 78A30

1. Introduction. Everybody has heard of the Faraday cage effect, whereby a wire mesh or metal screen serves to block electric fields and electromagnetic waves. Faraday reported his experiments with a twelve-foot mesh cube in 1836 [10][1], and engineers and physicists have used metal shielding to isolate circuits and systems ever since. A familiar example is the door of a microwave oven with its metal screen with holes. The screen keeps the microwaves from getting out while allowing light, with its much shorter wavelength, to pass through. Science museums sometimes dramatize the effect with electric sparks, as illustrated in Figure 1.1.

One would imagine that there must a standard mathematical analysis of electrostatic or electromagnetic screening to be found in physics and engineering textbooks, or at least in more specialized monographs, or in the journal literature. It seems that this is not so. There may be an analysis known to a specialized community somewhere, but we have consulted with enough people on this subject to be confident that no such treatment is widely known. The effect is mentioned in passing in some books, but usually with no equations. An impression is sometimes given that the strength of the effect is exponential or nearly exponential as a function of distance from the screen, a claim we have been unable to justify. One of the few mathematical treatments we have found is in Sec. 7-5 of v. 2 of *The Feynman Lectures on Physics* [11], where so far as we can tell, the analysis is incorrect. Feynman considers equal charges rather than equal potentials, his wires are of infinitesimal radius, there is no wavelength or indeed external field in his discussion, and the strength of the effect is predicted to be exponential.

We shall see that there is rapid convergence in the Faraday cage effect, but it is not what one might expect. As the wire spacing decreases, the field inside the cage

[1] The absence of field inside a continuous metal shell was noted by Benjamin Franklin as early as 1755 [13, §2-18].

FIG. 1.1. *Dramatization of the Faraday cage effect. This image shows the giant Van de Graaff generator at the Museum of Science in Boston. (Photo © Steve Marsel, courtesy of the Museum of Science, Boston.)*

converges rapidly not to zero, but to the solution of a homogenized problem involving a continuum boundary condition. Physically, the boundary condition expresses the property that the boundary has limited capacitance since it takes work to push charge onto small wires.

This paper analyzes the Faraday cage phenomenon from several points of view, and we do not want the reader to lose sight of the main results. Accordingly, the results are presented in relatively short sections 3–6, with some of the mathematical details deferred to Appendices A–C. The discrete model of Section 6 is simple enough to be used in teaching, and indeed, it was assigned to 70 Oxford graduate students in the course "Scientific Computing for DPhil Students" in November 2014.

We note that another paper about Faraday shielding has been published by Paul Martin after discussion with us about some of our results [16].

2. 2D electrostatic model. Our study focusses on a simple 2D electrostatic model, which we now describe.[2] Given a bounded simply connected open subset of the plane with smooth boundary Γ, suppose that n disks of radius r (representing the wires) are positioned along Γ at constant separation between neighboring disk centers (measured with respect to arc length along Γ). For convenience we will identify the x-y plane with the complex z-plane. Our primary example will be the case where Γ is the unit circle and the wires are situated at the nth roots of unity. An illustration

---

[2] We work throughout in dimensionless variables, scaling lengths with some typical cage dimension.
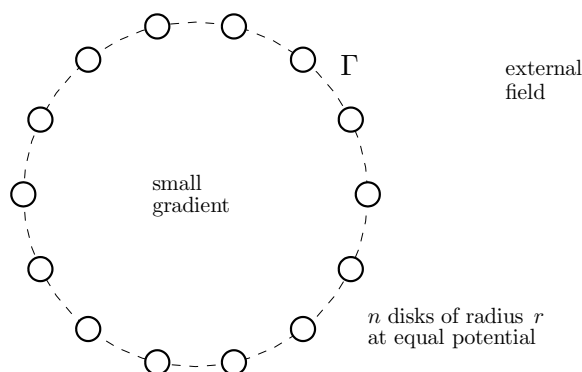
FIG. 2.1. *Model of the Faraday cage in 2D. The curve* Γ *on which the wires are located, in this case a circle, is shown as a dashed line.*

of the geometry in this case is given in Figure 2.1.

We seek a real function $\phi(z)$ that satisfies the Laplace equation

$$(2.1) \qquad\qquad \nabla^2 \phi = 0$$

in the region of the plane exterior to the disks, and the boundary condition

$$(2.2) \qquad\qquad \phi = \phi_0 \quad \text{on the disks.}$$

Equation (2.2) asserts that the disks are conducting surfaces at equal potential; here ϕ_0 is an unknown constant to be determined as part of the solution. We emphasize that (2.2) fixes $\phi(z)$ to a constant value on disks of finite radius $r > 0$. This is in contrast to some discussions of screening effects (e.g. [11, §7-5], [24, §7.5.1]) where the wires are supposed to have infinitesimal radius and are modelled as equal point charges. It is well known in harmonic function theory that Dirichlet boundary conditions can be imposed on finite-sized boundary components (the precise condition is that each boundary component must be a set of *positive capacity* [2]), but not at isolated points. Mathematically, the attempt to specify a potential at an isolated point will generally lead to a problem with no solution. Physically, one may imagine a potential fixed at an isolated point, but its effect will be confined to an infinitesimal region.

We also need to specify some external forcing and appropriate boundary conditions at infinity. Our numerical examples will focus on the case where the external forcing is due to a point charge of strength 2π located at the fixed point $z = z_s$ outside Γ, stipulating that

$$(2.3) \qquad\qquad \phi(z) = \log(|z - z_s|) + O(1) \quad \text{as } z \to z_s,$$

$$(2.4) \qquad\qquad \phi(z) = \log(|z|) + o(1) \quad \text{as } z \to \infty.$$

Equation (2.4) implies that the total charge on all the disks is zero, though the charge on each individual disk will in general be nonzero. Since the charge on a disk is equal to the integral of the normal derviative $\partial\phi/\partial\mathbf{n}$ around its boundary, (2.4) thus implies that the sum of these n integrals is zero. (Here $\mathbf{n}$ denotes the unit outward normal vector on a curve of integration.)

Our aim is to investigate quantitatively the behavior of the solution ϕ inside the cage, specifically the magnitude of the associated electric field, $\nabla\phi$, as a function of
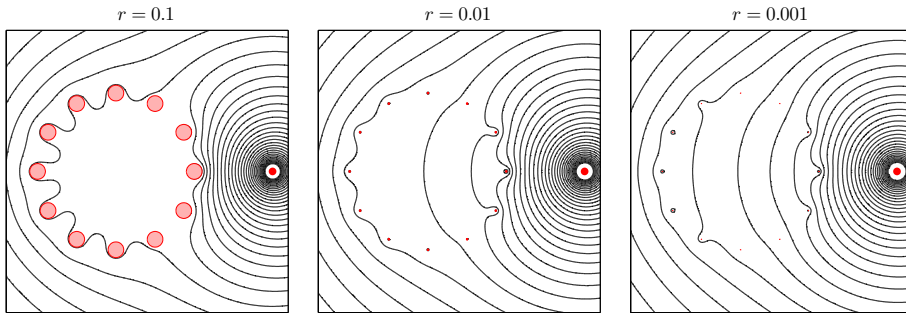
Fig. 3.1. *Dependence on the radius r for fixed number of disks $n = 12$. The equipotential curves visible correspond to values $\phi(z) = -2, -1.9, \ldots, 1.1, 1.2$. As $r \to 0$ the screening effect weakens slowly, with the field strength inside the cage growing in proportion to $|\log r|$. For these three configurations the gradients at the center are $|\nabla\phi(0)| \approx 0.012,\ 0.131,$ and 0.212; in the limit $r = 0$ it would be $|\nabla\phi(0)| = 1/2$. The constant potentials ϕ_0 on the wires are equal to $\log 2$ minus $3.32 \times 10^{-5},\ 2.05 \times 10^{-5},$ and 2.03×10^{-5}.*

TABLE 3.1
Computed values of $|\nabla\phi(0)|$ for various r and n. Entries marked "0" correspond to cases where the wires overlap, so the cage is a continuous shell and the shielding is perfect.

	$r = 10^{-1}$	10^{-2}	10^{-3}	10^{-4}	10^{-5}	10^{-6}
$n = 5$	0.1118	0.2663	0.3348	0.3723	0.3959	0.4122
10	0.0236	0.1582	0.2399	0.2902	0.3241	0.3486
20	0.0003	0.0699	0.1406	0.1916	0.2300	0.2598
40	0	0.0229	0.0693	0.1082	0.1406	0.1681
80	0	0.0047	0.0297	0.0539	0.0757	0.0954
160	0	0.0000	0.0112	0.0246	0.0372	0.0492
320	0	0	0.0036	0.0105	0.0173	0.0239

the number n and radius r of the wires. We present four methodologies for doing this: direct numerical calculation (Section 3), an analytical bound based on conformal mapping (Section 4), a homogenized approximation derived from the method of multiple scales (Section 5), and an approximation by point charges determined by solving a quadratic energy minimization problem (Section 6).

3. Numerical calculations. For our numerical calculations we compute solutions to the problem (2.1)–(2.4) accurate to many digits by the method of expansion in fundamental solutions of the Laplace equation with least-squares matching on the boundary. Details are given in Appendix A.

Figure 3.1 shows numerical results for the case where Γ is the unit circle and the forcing is by a point charge at $z_s = 2$, for fixed $n = 12$ and varying wire radii r. One sees that the screening effect weakens as $r \to 0$, and in the limit $r = 0$, there will be no screening at all. The dependence on r is logarithmic.

Figure 3.2 fixes $r = 0.01$ and varies n, showing results for $n = 10, 20, 40$. With each doubling of n, the field in the cage weakens, but only by approximately a factor of 2. This figure highlights the fact that in this model at least, the Faraday cage effect is not very strong.
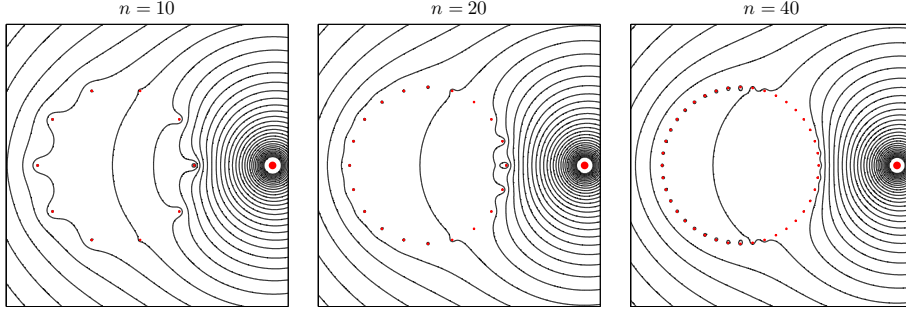
FIG. 3.2. *Dependence on the number of disks n for fixed radius r = 0.01. The screening improves only inverse-linearly as n increases, with the field strength inside the cage scaling like $O(n^{-1})$ for fixed r with $nr \ll 1$. The gradients at the center are $|\nabla\phi(0)| \approx 0.158,\ 0.070,$ and $0.023,$ and the potentials are $\log 2$ minus $9.8 \times 10^{-5},\ 4.9 \times 10^{-8},$ and approximately 2×10^{-14}.*
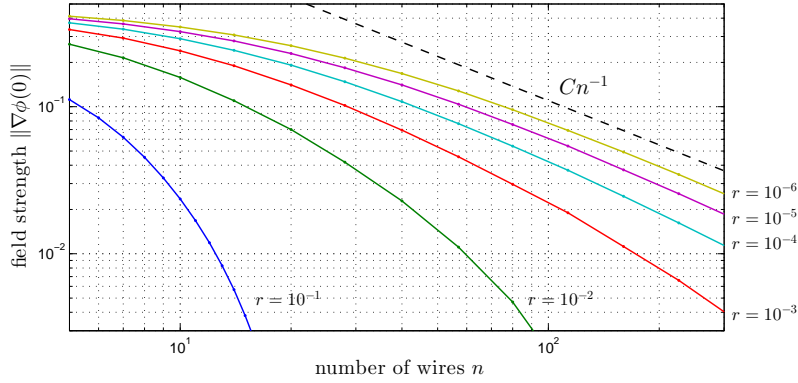

FIG. 3.3. *Graphical representation of data as in Figures 3.1 and 3.2: $|\nabla\phi(0)|$ as a function of n for various values of r. The top edge of the plot corresponds to the value $|\nabla\phi(0)| = 1/2$ one would get in the absence of shielding.*

Table 3.1 records numerically computed gradients $|\nabla\phi(0)|$ at the center of the disk for six values of r and seven values of n. In the absence of the cage, this quantity would take the value $1/2$. It is interesting to see that even when the radius is as small as 10^{-6}, the field is quite a bit weaker than this. Faraday cages have *some* effect even when the wires are extraordinarily thin. They don't bring the field strength strikingly close to zero, on the other hand, even when the wires are rather thick.

Figure 3.3 represents such data graphically. In the upper-right region of the plot, one sees that for large n and small r, the gradient decreases inverse-linearly with n. More precisely, one can observe empirically that for $n \gg 1$, $r \ll 10^{-3}$, $nr < 1$ and $|z_s| > 1$ one has

$$(3.1) \qquad\qquad |\nabla\phi(0)| \approx \frac{-2\log r}{n|z_s|}.$$

Thus the strength of the screening effect is linear in n, logarithmic in r, and linear in $|z_s|$. This observation is confirmed in Section 4 by a theorem and in Section 5 by a homogenized analysis, where a more precise formula is given as equation (5.14).

Our cage has wires of equal radius and spacing, but this is not essential. Numerical experiments confirm that if the radii and positions are perturbed by small amounts,

the fields do not change very much.

4. Theorem. By combining known bounds for harmonic functions with certain conformal transplantations, it is possible to derive a theorem that confirms the numerical observation (3.1). Rather than restrict attention to the specific forcing function $\log(|z - z_s|)$, we now imagine a Faraday cage on the unit circle subject to an arbitrary forcing field outside the disk of radius $R > 1$. Specifically, given $R > 1$, let ϕ be a harmonic function satisfying $|\phi(z)| < 1$ in the region $|z| < R$ minus the n disks of radius r, where it takes the constant value $\phi(z) = 0$. Appendix B establishes the following bound.

Theorem 1. *Given $R > 1$, $n \geq 4$, and $r \leq 1/n$, let ϕ be a harmonic function satisfying $|\phi(z)| \leq 1$ in the region Ω consisting of the disk $|z| < R$ punctured by the n disks of radius r centered at the nth roots of unity, where ϕ takes a constant value ϕ_0 between -1 and 1. Then*

$$(4.1) \qquad |\nabla \phi(0)| \leq \frac{4|\log r|}{n \log R}.$$

Although this theorem as stated gives a bound on the gradient just for $z = 0$, the argument can be extended to a similar bound for any z with $|z| < 1 - r$, with constants weakening by a factor proportional to $(1 - r - |z|)^{-1}$. We note also that although the theorem gives a bound of order $1/\log R$ for large R, the actual scaling is smaller than this, of order $1/R$, as in (3.1).

5. Continuum approximation. In Figures 3.1–3.2 it is evident that inside the Faraday cage, though the potential is not very close to a constant, it is close to *some* smooth function, except just next to the wires. Under appropriate assumptions, one can make this observation precise, approximating the cage by a continuum model with an effective boundary condition on the curve Γ. Details of our derivation by the method of multiple scales are given in Appendix C. Related effective boundary conditions have been obtained for problems with discontinuities along layers by the method of "generalized impedance boundary conditions" as discussed for example in [3, 9, 21]. The closest treatment we know of to our own is that of Delourme et al. [6, 7, 8].

The homogenized approximation can be described as follows. Suppose the constant separation between neighboring wire centers (measured with respect to arc length along Γ) is $\varepsilon = |\Gamma|/n \ll 1$, where $|\Gamma|$ is the total arc length, and the radius of each wire is $r \ll \varepsilon$. The crucial scaling parameter that determines the effectiveness of the screening is

$$(5.1) \qquad \alpha = \frac{2\pi}{\varepsilon \log(\varepsilon/2\pi r)}.$$

If $\varepsilon \gg 1/\log(\varepsilon/r)$, then $\alpha \ll 1$ and the wires are too thin for effective screening. If $\varepsilon \ll 1/\log(\varepsilon/r)$, then $\alpha \gg 1$ and the screening is strong. Specifically, here is the continuum problem that results from our asymptotic analysis. Away from Γ, the leading order solution satisfies the Laplace equation. On Γ, ϕ is continuous, but its normal derivative satisfies a jump condition:

$$(5.2) \qquad \left[\frac{\partial \phi}{\partial \mathbf{n}}\right] = \alpha(\phi - \phi_0) \quad \text{on } \Gamma,$$
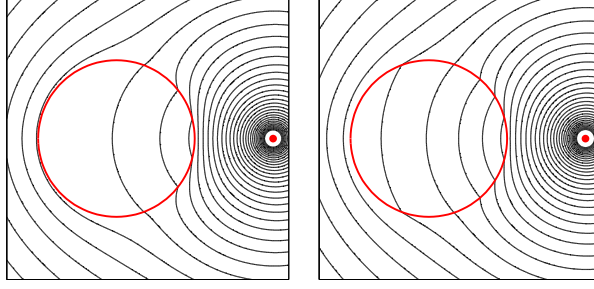
Fig. 5.1. *Analogue of Figure 3.1 for the continuum approximation determined by (5.1) and (5.5)–(5.9). Again the number of disks is fixed at $n = 12$ and the radius r varies. Note the striking agreement of the two images shown with those of Figure 3.1, corresponding to values $\alpha = 5.660$ and 2.713. The first image is absent because in this case $rn > 1$, making α negative and the homogenized approximation inapplicable. The mean potential ϕ_0 of (5.7) is $\log 2 \approx 0.693$.*

where ϕ_0, to be determined, is the mean value of ϕ on Γ. Here $[f]$ denotes the jump in f across Γ, from exterior to interior, and $\mathbf{n}$ is the unit outward normal vector on Γ. Note that for $\alpha \ll 1$, (5.2) implies that $\partial\phi/\partial\mathbf{n}$ barely jumps across Γ: the screening is weak. For $\alpha \gg 1$, (5.2) implies that ϕ is almost constant along Γ: the screening is strong.

Equation (5.2) can be given a physical interpretation, if we recall that across a curve supporting a charge distribution of density ρ, the gradient of a potential jumps by ρ. Thus another way to write (5.2) is

$$(5.3) \qquad \rho = \alpha(\phi - \phi_0) \ \text{ on } \Gamma,$$

where ρ, a function of z, is the charge density along Γ. The parameter α, a ratio of charge to voltage, can be interpreted as a capacitance per unit length. For a perfect shell with $\alpha = \infty$, ρ is such that $\phi = \phi_0$ along Γ, so the external field is exactly cancelled, but for finite α, ρ does not adjust so far.

Solving for r in (5.1) gives

$$(5.4) \qquad r = \frac{\varepsilon}{2\pi} e^{-2\pi/\alpha\varepsilon}.$$

In other words, the distinguished limit in which α is strictly of order one occurs when $r \sim \varepsilon A \exp(-c/\varepsilon)$ as $\varepsilon \to 0$ for some constants $A, c > 0$ (in which case $\alpha \sim 2\pi/c$). Essentially the same critical scaling is derived in [19, 20] for problems of electrostatic screening and by rigorous homogenization theory in [5] in the context of a much more general discussion of limiting behavior of solutions of partial differential equations in domains with microstructure.

For the cage subject to a point charge as in Section 2, the homogenized model takes the following form:

$$(5.5) \qquad \nabla^2\phi = 0 \ \text{ in } \mathbb{R}^2 \setminus \{\Gamma \cup z_s\},$$

$$(5.6) \qquad [\phi] = 0 \ \text{ on } \Gamma,$$

$$(5.7) \qquad \left[\frac{\partial\phi}{\partial\mathbf{n}}\right] = \alpha(\phi - \phi_0) \ \text{ on } \Gamma,$$
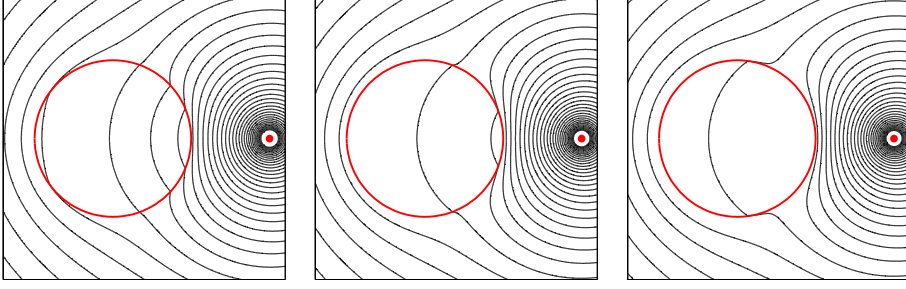
Fig. 5.2. *Analogue of Figure 3.2 for the continuum approximation determined by (5.1) and (5.5)–(5.9). Now the radius is fixed at $r = 0.01$ and the number of disks n varies. Again note the agreement with the discrete case. The values of α for these three figures are 4.343, 12.43, and 43.65, and the mean potential ϕ_0 is again $\log 2$.*

TABLE 5.1

Approximations to the data of Table 3.1 by the continuum model (5.14). For $n > 5$ and $r < 10^{-2}$ there is close agreement. Entries marked " - " correspond to values $\alpha < 0$ in (5.1), where the continuum model is inapplicable.

	$r = 10^{-1}$	10^{-2}	10^{-3}	10^{-4}	10^{-5}	10^{-6}
$n = 5$	0.1085	0.2726	0.3397	0.3762	0.3992	0.4150
10	-	0.1577	0.2397	0.2901	0.3241	0.3486
20	-	0.0693	0.1406	0.1916	0.2300	0.2598
40	-	0.0219	0.0693	0.1082	0.1406	0.1681
80	-	0.0028	0.0297	0.0539	0.0756	0.0954
160	-	-	0.0112	0.0246	0.0372	0.0492
320	-	-	0.0035	0.0105	0.0173	0.0239

$$(5.8) \qquad \phi(z) = \log(|z - z_s|) + O(1) \ \text{ as } z \to z_s,$$

$$(5.9) \qquad \phi(z) = \log(|z|) + o(1) \ \text{ as } z \to \infty.$$

For the particular case of the unit circle, (5.5)–(5.9) can be solved explicitly to give

$$(5.10) \qquad \phi_0 = \log(|z_s|),$$

independently of α, and

$$(5.11) \quad \phi(z) = \log(|z - z_s|) + \begin{cases} \displaystyle\sum_{m=1}^{\infty} \frac{\alpha |z|^m \cos m(\arg z - \arg z_s)}{m(\alpha + 2m)|z_s|^m}, & |z| \leq 1, \\[3mm] \displaystyle\sum_{m=1}^{\infty} \frac{\alpha |z|^{-m} \cos m(\arg z - \arg z_s)}{m(\alpha + 2m)|z_s|^m}, & |z| \geq 1. \end{cases}$$

Figures 5.1 and 5.2 show the resulting approximations, closely matching Figures 3.1 and 3.2. To make the comparison quantitative, we calculate that the gradient at the center of the cage has amplitude

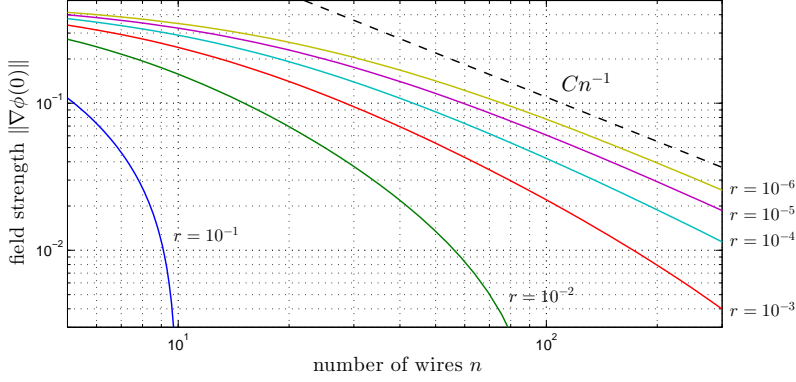$$(5.12) \qquad |\nabla \phi(0)| = \frac{2}{(\alpha + 2)|z_s|}.$$

FIG. 5.3. *Analogue of Figure* 3.3, *with data now corresponding to the continuum model* (5.14).

Since $\varepsilon = 2\pi/n$ and $r/\varepsilon = rn/2\pi$, (5.1) becomes

$$(5.13) \qquad \alpha = \frac{n}{\log(1/rn)},$$

from which it follows that (5.12) can be written

$$(5.14) \qquad |\nabla\phi(0)| = \frac{1}{|z_s|} \frac{1}{1 + n/(2\log(1/rn))}.$$

Comparison of Tables 5.1 and 3.1 and of Figures 5.3 and 3.3 shows that (5.14) is a very accurate approximation indeed. This formula also confirms (3.1), with the two expressions being asymptotic to each other in the limit $n \to \infty$, $rn \to 0$.

Our homogenized analysis does not depend on the geometry of the cage being uniform. If the radius and/or the spacing of the wires varies around the cage, then the homogenized model should still give a good approximation, now with α as a function of position.

6. A cage of point charges. Unlike point potentials, point charges make good sense mathematically and physically. An exponentially effective cage can be made from point charges; the only difficulty is that the required charge distribution is not the one induced in a Faraday cage.

To explain this observation, we first present two further variants of Figures 3.2 and 5.2. First, consider Figure 6.1. Here we take the smooth charge distribution of Figure 5.2 and discretize it in point charges. To be precise, at each of n points on the unit circle, we sample the smooth charge density resulting from the homogenized model and multiply the result by $2\pi/n$; we take this number as the amplitude of a charge at this point. The picture looks virtually the same as in Figure 3.2. This reflects the phenomenon that the trapezeoidal rule in equispaced points on a circular contour is exponentially accurate when applied to an analytic function [23]. The potential functions ϕ of Figure 5.2 can be written as integrals over the circle; in Figure 6.1 the integrals have been replaced by discrete trapezoidal approximations.

Figure 6.2 shows the same configuration, except based on the discretization of a different charge distribution: that induced on a perfectly conducting circular shell, i.e., the limit $\alpha = \infty$ in the last section (readily determined by the method of images). Now the field inside is exponentially close to zero, as many, including initially ourselves,
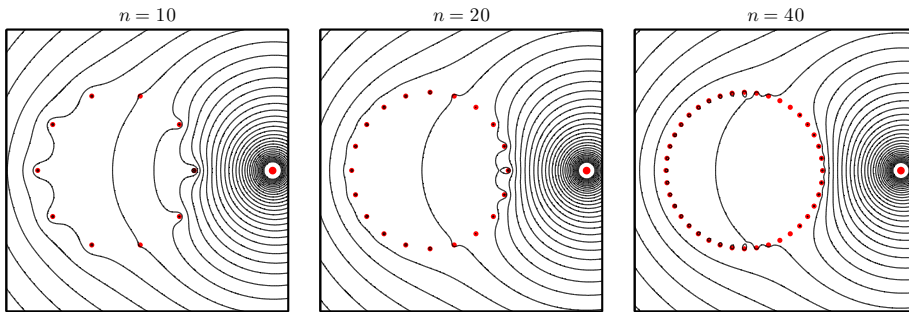
FIG. 6.1. *Point charges approximation to a Faraday cage. The images show the potentials associated with* 10, 20, *or* 40 *point charges with strengths obtained by discretizing the continuous charge distributions of Figure* 5.2. *The gradients at the center are* $|\nabla\phi(0)| \approx 0.157, 0.069,$ *and* 0.022. *Nearly the same images and numbers are obtained by solving the quadratic optimization problem* (6.4).
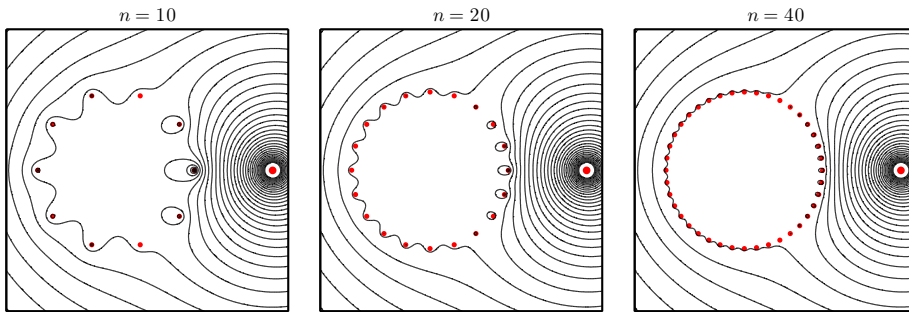

FIG. 6.2. *Much better shielding achieved by different point charges, derived by discretizing the charge distribution of a perfect circular conductor. The gradients at the center are* $|\nabla\phi(0)| \approx 2.444 \times 10^{-3}, 2.384 \times 10^{-6},$ *and* $2.274 \times 10^{-12},$ *with exponential convergence to zero as* $n \to \infty$. *Unfortunately, this is not the charge distribution induced in an actual Faraday cage.*

would imagine a Faraday cage must work. Again one can interpret the effect as exponential convergence of the periodic equispaced trapezoidal rule.[3]

The consideration of point charges suggests a new model of the Faraday cage that reduces it to a problem of linear algebra; the flavor is related to that of [1]. We have seen that what limits the effectiveness of a cage is the limited-capacitance effect stemming from the work required to put charge on a small wire. Specifically, the energy associated with charge of amplitude q on a disk of radius r is $-(q^2/2)\log r$. Suppose now that we have n disks of radius r centered at the points z_k loaded with charges q_k and in the presence of an external field $\log|z - z_s|$. For $r \ll \min|z_k - z_j|$, the energy of this configuration is

$$(6.1) \qquad E(\mathbf{q}) = -\frac{1}{2}\sum_{k=1}^{n} q_k^2 \log r - \sum_{k=1}^{n}\sum_{j>k} q_k q_j \log|z_k - z_j| - \sum_{k=1}^{n} q_k \log|z_k - z_s|,$$

where $\mathbf{q} = (q_1, \dots q_n)^T$: the three terms correspond to self-energy of the disks, interactions between disks, and interactions with the external field. We further know that

---

[3]If the wires are not equally spaced, such an interpretation is still valid provided one generalizes the trapezoidal formula appropriately via trigonometric interpolation [23, Section 9].

the total charge on all the wires is zero,

$$(6.2) \qquad \sum_{k=1}^{n} q_k = 0.$$

This formulation suggests that we can find the charges q_k by minimizing the quadratic form $E(\mathbf{q})$ over all n-vectors $\mathbf{q}$ satisfying (6.2). This is a constrained quadratic programming problem of the form

$$(6.3) \qquad E(\mathbf{q}) = \frac{1}{2}\mathbf{q}^T A \mathbf{q} - \mathbf{f}^T \mathbf{q}, \qquad \mathbf{c}^T \mathbf{q} = 0,$$

for a suitable matrix A and vectors $\mathbf{f}$ and $\mathbf{c}$, with solution vector $\mathbf{q}$ satisfying the block 2×2 linear system

$$(6.4) \qquad \begin{pmatrix} A & \mathbf{c} \\ \mathbf{c}^T & 0 \end{pmatrix} \begin{pmatrix} \mathbf{q} \\ \lambda \end{pmatrix} = \begin{pmatrix} \mathbf{f} \\ 0 \end{pmatrix};$$

here λ is a Lagrange multiplier. Solving (6.4) for $\mathbf{q}$ leads to a cage of point charges whose potentials look essentially the same as in Figures 3.2 and 6.1 (not shown).

7. Discussion. This article has investigated an electrostatic problem. Our analysis shows that the shielding improves only linearly as the spacing between wires of a cage shrinks, and this is probably why your cell phone often works inside an elevator. The shielding also depends on having wires of finite thickness, and this is probably why it is hard to see into your microwave oven. (If thin wires provided good enough shielding, the designers of microwave oven doors would use them.) Bjorn Engquist has pointed out to us an amusing illustration of the challenges of Faraday shielding that combines both of these devices. Put your cell phone inside your microwave oven, close the door, and give it a call. The phone will ring merrily!

In particular, we have found that the Faraday shielding effect can be accurately modeled by a homogenized problem with a continuous boundary condition, which expresses the fact that the boundary has limited capacitance since it takes work to force charge onto narrow wires. This capacitance observation in turn suggests even simpler models based on energy minimization. We presented such a model in a discrete context in Section 6, and a continuous argument of limited capacitance and energy minimization could also be developed.

The overall structure of our arguments is summarized in Figure 7.1. Let us quickly mention yet another argument, suggested by Toby Driscoll, that explains in still another way that Faraday shielding must be weak. Consider the configuration of a circular shell that is complete except for a single gap of size ε. By a conformal map, one can calculate the potential inside this shell exactly, and the gradient in the interior comes out of magnitude $O(\varepsilon^2)$. Clearly the cage of n gaps will have weaker screening than this screen of one gap: weaker, as we have seen, by a factor $O(\varepsilon^{-1})$ corresponding to the number of gaps.

It has surprised us deeply in the course of this work to find no mathematical analysis of the Faraday cage effect in the literature, despite its age, fame, and practical importance. Feynman's treatment alone must have been read by tens of thousands of students and physicists, which may have contributed to the widespread misconception that the shielding is exponential. Curiously, Maxwell in his 1873 treatise considered the same special case of an infinite planar array of wires and got it right, including the
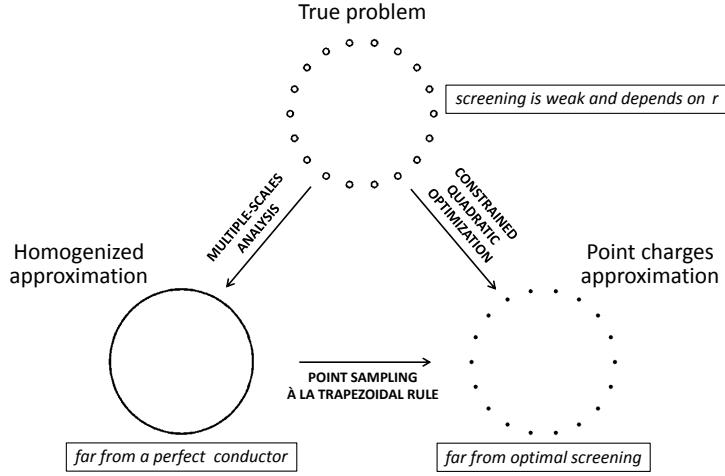
True problem

screening is weak and depends on r

MULTIPLE-SCALES ANALYSIS

CONSTRAINED QUADRATIC OPTIMIZATION

Homogenized approximation

Point charges approximation

POINT SAMPLING
À LA TRAPEZOIDAL RULE

far from a perfect conductor

far from optimal screening

FIG. 7.1. *Schematic summary of the arguments of this paper. The optimization model, based on energy minimization for a surface of limited capacitance, could also be formulated in a continuous setting.*

dependence on radius r [17]. However, we are unaware of any follow-up of Maxwell's work.

For electromagnetic waves, the shielding as a rule will be weaker. It is intuitively clear that one must expect this when the wavelengths are much less than the mesh spacing, but even for longer wavelengths, which one might at first think could not penetrate the cage, the shielding may be weak because of resonance. For example, suppose (2.1)–(2.4) are replaced by a Helmholtz equation system

$$(7.1) \qquad\qquad \nabla^2 \phi + \omega^2 \phi = 0,$$

$$(7.2) \qquad\qquad \phi(z) = \phi_0 \;\; \text{on the disks,}$$

$$(7.3) \qquad\qquad \phi(z) = \log(|z - z_s|) + O(1) \;\; \text{as } z \to z_s,$$

$$(7.4) \qquad\qquad \text{outgoing radiation condition} \;\; \text{as } z \to \infty.$$

(This is a rather nonstandard Helmholtz problem in that ϕ_0 is not fixed but unknown, to allow for direct comparison with the electrostatic problem. The formulation can be completed with a condition analogous to the zero-total-charge property implied by (2.4). For our calculations we require the coefficients d_j of Hankel function contributions $d_j H_0(\omega|z - c_j|)$ to sum to zero in analogy to the condition imposed for the electrostatic case in Appendix A.) Equations (7.1)–(7.4) could be obtained after separation of variables $u(z,t) = \exp(-i\omega t)\phi(z)$ by considering the wave equation $\partial^2 u/\partial t^2 = \nabla^2 u$ subject to oscillatory forcing $u(z,t) = \exp(-i\omega t)\log(|z - z_s|) + O(1)$ as $z \to z_s$ with $u(z,t) = e^{-i\omega t}\phi_0$ on the disks. If ω is small enough, then (2.1)–(2.4) and (7.1)–(7.4) will lead to much the same solutions, with similar shielding properties. If ω is close to a zero of a Bessel function J_ν for integer ν, however, corresponding to
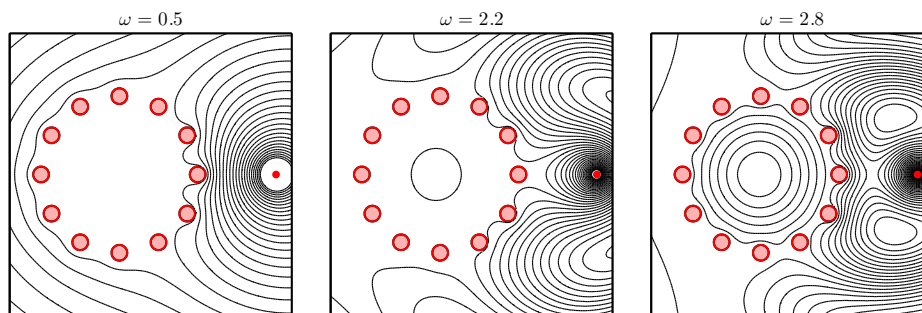
FIG. 7.2. *Repetition of the first panel of Figure* 3.1 *for the Helmholtz problem* (7.1)–(7.4) *for three values of* ω. *Level curves of* $Re(\phi(z))$ *are shown with levels at* $-2, -1.9, \ldots, 1.2$ *as in Figure* 3.1. *For* $\omega = 2.8$, *there is an approximate resonance inside the cage and a significant field there.*

an eigenmode of the Laplacian in the unit disk, then a large response may be stimulated within the cage, even if the wavelength is bigger than the mesh spacing. For example, Figure 7.2 shows results in the same format as the first image of Figure 3.1 for $\omega = 0.5$, 2.2, and 2.8. For the small value of ω, the image looks approximately as before. As ω increases, waves of wavelength $\omega/2\pi$ appear. The image for $\omega = 2.8$ shows a hint of the resonance that would appear in the case of a perfect unit circle at $\omega \approx 2.405$; with larger n and smaller r these numbers would match more closely.

This Helmholtz equation model is highly simplified. A proper discussion of the electromagnetic case, which is beyond the scope of this paper, must consider different polarizations of electromagnetic waves. For example, a wave with electric field parallel to an array of parallel wires will behave differently from a wave with electric field perpendicular to such an array. Early studies of diffraction of electromagnetic waves by wire arrays include [4, 15, 18], and indeed such questions go back to Hertz, J. J. Thomson, Lord Rayleigh, and Lamb (who charmingly refers to "electric waves") [14]. For time-dependent problems, moreover, other effects become relevant including finite resistivity, skin depth, and electromagnetic induction. In the field of electromagnetic screening it is well recognized that a finite amplitude wave may propagate through a screen, not just an evanescent one.

For a wire cage in three dimensions, electrostatic shielding will be much as we have described here for a 2D problem. Again the strength of the shielding will be linear in the mesh spacing, logarithmic in the radius. A mesh with wires aligned orthogonally in both directions will shield better than a mesh with wires aligned in just one direction, but the improvement will be by less than a factor of 2. (We continue to assume that all wires are electrically connected so that they lie at the same potential.) A continuum model can be derived as before; the jump condition (5.2) will be applied across the bounding surface with α changed to 2α.

Finally, we return to the dramatization of Figure 1.1. Effects of sparking and lightning involve more than just Faraday screening: the ionization of the air is non-linear and nucleates at points of strong field, typically near sharp corners or other small-scale features, as has been well known since Franklin invented the lightning rod. Indeed, whereas for our electrostatic model problem thinner wires provide weaker shielding, perhaps one might in principle devise a cage whose properties as a lightning rod would be the reverse: thin wires might make for better lightning protection than thicker ones, because of sparking ionization more readily.

```
% Solve the problem:
  n = 12; r = 0.1;                         % number and radius of disks
  c = exp(2i*pi*(1:n)/n);                  % centers of the disks
  rr = r*ones(size(c));                    % vector of radii
  N = max(0,round(4+.5*log10(r)));         % number of terms in expansions
  npts = 3*N+2;                            % number of sample points on circles
  circ = exp((1:npts)'*2i*pi/npts);        % roots of unity for collocation
  z = []; for j = 1:n
    z = [z; c(j)+rr(j)*circ]; end          % collocation points
  A = [0; -ones(size(z))];                 % the constant term
  zs = 2;                                  % location of the singularity
  rhs = [0; -log(abs(z-zs))];              % right-hand side
  for j = 1:n
    A = [A [1; log(abs(z-c(j)))]];         % the logarithmic terms
    for k = 1:N
      zck = (z-c(j)).^(-k);
      A = [A [0;real(zck)] [0;imag(zck)]]; % the algebraic terms
    end
  end
  X = A\rhs;                               % solve least-squares problem
  e = X(1); X(1) =[];                      % constant potential on wires
  d = X(1:2*N+1:end); X(1:2*N+1:end) = []; % coeffs of log terms
  a = X(1:2:end); b = X(2:2:end);          % coeffs of algebraic terms

% Plot the solution:
  x = linspace(-1.4,2.2,120); y = linspace(-1.8,1.8,120);
  [xx,yy] = meshgrid(x,y); zz = xx+1i*yy; uu = log(abs(zz-zs));
  for j = 1:n
    uu = uu+d(j)*log(abs(zz-c(j)));
    for k = 1:N, zck = (zz-c(j)).^(-k); kk = k+(j-1)*N;
      uu = uu+a(kk)*real(zck)+b(kk)*imag(zck); end
  end
  for j = 1:n, uu(abs(zz-c(j))<rr(j)) = NaN; end
  z = exp(pi*1i*(-50:50)'/50);
  for j = 1:n, disk = c(j)+rr(j)*z; fill(real(disk),imag(disk),[1 .7 .7])
    hold on, plot(disk,'-r'), end
  contour(xx,yy,uu,-2:.1:1.2), colormap([0 0 0]), axis([-1.4 2.2 -1.8 1.8])
  axis square, plot(real(zs),imag(zs),'.r')
```

FIG. A.1. *Example program for computing the field inside the Faraday cage, with the variable u used for ϕ in the text and e for ϕ_0. This code produces the first image of Figure 3.1 in a fraction of a second on a desktop computer.*

This investigation originated in the third author's study with J. A. C. Weideman of the exponential convergence of the periodic trapezoidal rule for analytic functions [23]. Surely, we imagined, a Faraday cage must provide exponential shielding for the same mathematical reasons as the trapezoidal rule provides exponential convergence? Eventually we realized that the analogy is not so straightforward.

Appendix A. Numerical method. Figures 3.1–3.3 and Table 3.1 report numerical results for the Laplace problem (2.1)–(2.4). These results were calculated by a method of expansion in appropriate basis functions with least-squares matching on the boundary. In principle, this method converges exponentially as a function of the number of parameters employed, and in practice, it is not hard to get several digits of accuracy provided one is careful to avoid parameter regimes where the matrices are highly ill-conditioned. The method is sometimes associated with the name of Mikhlin, and our own calculations were based on adaptations of codes given in [22].

Let $\{c_j\}$ denote the centers of the n wires, each with radius r. The expansion we

utilize takes the form

$$\text{(A.1)} \quad \phi(z) = \log|z - z_s| + \sum_{j=1}^{n} \left\{ d_j \log|z - c_j| + \text{Re}\left[\sum_{k=1}^{N} (a_{jk} - ib_{jk})(z - c_j)^{-k} \right] \right\},$$

where $\{d_j\}$, $\{a_{jk}\}$, and $\{b_{jk}\}$ are real constants to be determined along with $e = \phi_0$, the constant voltage on the wires in (2.2)). We fix d_1 by the condition $\sum d_j = 0$, which is equivalent to (2.4), and the rest of the parameters are unknowns. The number N is taken large enough for good accuracy but not so large as to make the matrices too ill-conditioned (especially an issue when r is small): our experimentally derived rule of thumb is to take N as the nonnegative integer closest to $4 + 0.5\log_{10}(r)$. For any coefficients, the function (A.1) satisfies (2.1), (2.3) and (2.4), and our aim is to find coefficients so that it also satisfies (2.2). To this end, the boundary of each disk is discretized in a number of points, typically $3N + 2$, which makes (2.2) into an overdetermined linear system of equations involving a matrix of dimension $(3nN+2n+1) \times (2nN+n+1)$. This problem is then solved by the standard methods invoked by the MATLAB backslash command. A sample MATLAB code is listed in Figure A.1.

For the Helmholtz equation of Section 7, the computations are similar but based on Hankel functions of the first kind $H_j^{(1)}$ rather than logarithms and inverse powers.

Appendix B. Proof of Theorem 1. To begin the proof, assume $\phi_0 = 0$. Under this assumption we claim that ϕ satisfies

$$\text{(B.1)} \quad |\phi(\zeta)| \leq \frac{|\log r|}{n \log R}, \quad |\zeta| \leq 1, \ \zeta \in \Omega.$$

To prove this, we note that for each $\zeta \in \Omega$, $\phi(\zeta)$ is a weighted average of the values of $\phi(z)$ on the boundary $\partial\Omega$; the weighting function is known as the *harmonic measure* associated with the point ζ. It follows that for any $\zeta \in \Omega$, the largest value that $|\phi(\zeta)|$ may take under the given assumptions on the boundary data is equal to the value taken by $\phi(\zeta)$ in the case where $\phi(z) = 1$ identically for $|z| = R$. (Equivalently, it is the harmonic measure of the boundary circle $|z| = R$ for the given ζ and Ω.) We can estimate this number by making use of the transformation $v = z^n$ followed by $w = (v - 1)/(1 - R^{-2n}v)$, as indicated in Figure B.1:

$$\text{(B.2)} \quad w = \frac{z^n - 1}{1 - R^{-2n}z^n}.$$

Under this transformation, the solution $\phi(w)$ to the Dirichlet problem in the region on the right of the figure corresponds pointwise to the solution in the left region, $\phi(z)$. (We abuse notation slightly by using the same symbol ϕ in the z, v, and w domains.) The region on the right is bounded on the outside by the circle $|w| = R^n$, with $\phi(w) = 1$, and on the inside by a curve S that is approximately the circle $\{w : |w| = rn\}$, with $\phi(w) = 0$. The minimal absolute value of points $w \in S$ is the value corresponding to $z = 1 - r$,

$$\text{(B.3)} \quad |w|_{\min} = \frac{1 - (1 - r)^n}{1 - R^{-2n}(1 - r)^n},$$

and an easy estimate using the assumption $r < 1/n$ gives

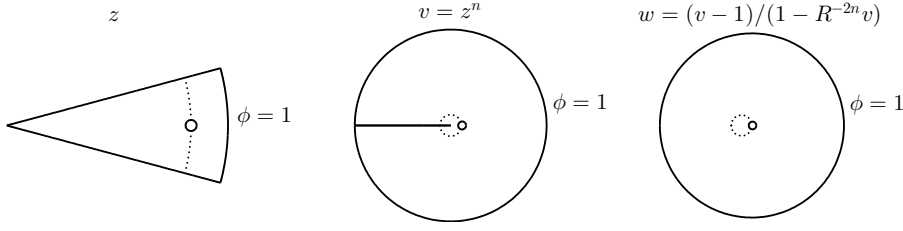$$|w|_{\min} \geq \frac{rn}{2}.$$

FIG. B.1. *Conformal transplantations of the harmonic function ϕ for the proof of Theorem 1. The left image shows one of n equal segments of the disk $|z| \leq R$ in the z-plane, a slice of cheese that omits the disk of radius $r \ll 1$ around $z = 1$; the dotted curve marks a portion of the unit circle. The middle image shows the result after the transformation $v = z^n$, giving an outer circle now of radius $|v| = R^n$; the omitted region is now approximately the disk about $v = 1$ of radius nr. The slit along $[-R^n, 0]$ can be removed since ϕ satisfies a homogeneous Neumann condition on both sides. The right image shows the result after a further adjustment by the Möbius transformation $w = (v - 1)/(1 - R^{-2n}v)$, which leaves the outer circle fixed at $|w| = R^n$ and moves the omitted near-disk to approximately the disk of radius nr about $w = 0$.*

It follows that $|\phi(w)|$ is bounded above by the value it would take if S were the circle about $w = 0$ of radius $rn/2$,

$$(B.4) \qquad |\phi(w)| \leq \frac{\log(2|w|/rn)}{\log(2R^n/rn)} = \frac{|\log r| + \log(2|w|/n)}{n \log R + \log(2/rn)}.$$

Equation (B.2) can be rewritten with z replaced by ζ as

$$w = -1 + \frac{1 - R^{-2n}}{\zeta^{-n} - R^{-2n}},$$

which implies that for $|\zeta| \leq 1$, $|w| \leq 2$. Therefore (B.4) implies

$$(B.5) \qquad |\phi(\zeta)| \leq \frac{|\log r| + \log(4/n)}{n \log R + \log(2/rn)}, \quad |\zeta| \leq 1.$$

Now since $n \geq 4$, $\log(4/n) \leq 0$, and since $r \leq 1/n$, $\log(2/rn) \geq 0$. Therefore this equation implies (B.1), as claimed.

Still with the assumption $\phi_0 = 0$, we now have a bound on $|\phi(\zeta)|$ for points $\zeta \in \Omega$ with $|\zeta| \leq 1$, and in particular on the disk $|\zeta| \leq 1 - r$. According to a standard result in harmonic function theory, it follows that $|\nabla\phi(0)|$ satisfies the same bound, except weakened by the factor $4/\pi(1 - r)$ [2, p. 125]:

$$(B.6) \qquad |\nabla\phi(0)| \leq \frac{4}{\pi(1 - r)} \frac{|\log r|}{n \log R}.$$

The proof is complete except that we must remove the assumption $\phi_0 = 0$ and allow ϕ_0 to take any value in $[-1, 1]$. We can do this by subtracting the constant ϕ_0 from the solution of the problem as stated in the theorem. This gives us a problem of the same form as before, but with boundary data potentially as large as 2 rather than 1; the gradient $\nabla\phi$ is not affected by the subtraction of a constant. Thus for arbitrary $\phi_0 \in [-1, 1]$, (B.6) holds except with 4 doubled to 8. Since $8/\pi(1-r) < 4$ for $r \leq 1/4$, this establishes (4.1). ∎

The reader may note that if $R < 1 + r$, the picture of Figure B.1 is invalid: the omitted disk around $z = 1$ extends outside the circle $|z| = R$. The argument given

remains valid, nevertheless, with Ω now defined as that portion of the disk $|z| < R$ that is disjoint from the n disks of radius r centered at the nth roots of unity.

Appendix C. Derivation of homogenized equation. Our method is multiple scales analysis, as described for example in [12]. We present the analysis for a vertical line of circular disks of radius $r = \delta\epsilon$, $\delta \ll 1$, centered on the straight line $x = 0$ at the points $(0, k\epsilon)$ for $k \in \mathbb{Z}$. The generalisation to an arbitrary curve is straightforward. Addition of a constant to the potential does not change the problem significantly, so for simplicity we look for a solution ϕ that is zero on the disks.

There are three asymptotic regions that make up the solution. First, there is an *outer region* away from the cage, in which $x = O(1)$. This region will see the cage as an effective boundary condition, leading to the problem (5.5)–(5.9). Second, there is a *boundary layer region*, in which $x = O(\epsilon)$. In this region the discrete nature of the wires becomes apparent, but they are of vanishing thickness and act as point charges. The solution here is of multiple-scales form in y, with fast scale $O(\epsilon)$ and slow scale $O(1)$. Third, there is an *inner region* near a single wire, in which $x = O(\delta\epsilon)$, $y = O(\delta\epsilon)$. This region determines the induced charge on the wire resulting from the equipotential condition.

The multiple scales form of the solution in y means that it is written in terms of a slow variable y and a fast variable $Y = y/\epsilon$, which are treated as independent. The extra freedom this gives is then removed by imposing the condition that the solution is exactly periodic (with unit period) in the fast variable Y. In fact, the slow variable y is carried simply as a parameter in the boundary layer and inner regions (it is relevant only in the outer region). To simplify the presentation we hide this dependence of the solution in these regions on y.

We consider the inner and boundary layer solutions in turn, before matching the expansions to determine the effective boundary condition on the outer solution.

Inner region. Rescaling near the wire at the origin by setting $(x, y) = (\delta\epsilon\xi, \delta\epsilon\eta)$ gives

$$\phi_{\xi\xi} + \phi_{\eta\eta} = 0 \qquad \text{for } \xi^2 + \eta^2 > 1,$$

with

$$\phi = 0 \qquad \text{on } \xi^2 + \eta^2 = 1.$$

The relevant solution is

$$\phi = A \log(\xi^2 + \eta^2)^{1/2}, \tag{C.1}$$

for some constant A.

Boundary layer region. In the boundary layer region we rescale $(x, y) = (\epsilon X, \epsilon Y)$ to give

$$\phi_{XX} + \phi_{YY} = 2\pi C \delta(X, Y) \quad \text{for } -1/2 < Y < 1/2, \tag{C.2}$$

with

$$\phi_Y = 0 \quad \text{on } Y = \pm 1/2, \tag{C.3}$$

where δ is the Dirac delta function. Here the constant C represents the induced charge on the wire, which will be determined by matching with the inner solution.

The boundary condition (C.3) is equivalent to imposing periodicity in the fast variable Y with unit period. The relevant solution to (C.2)–(C.3) is

$$(C.4) \qquad \phi = B + C \operatorname{Re}(\log \sinh(\pi Z)), \quad \text{where } Z = X + iY.$$

The constant B will also be determined by matching.

Matching between the inner and boundary layer regions. Written in terms of (X, Y) the inner solution (C.1) is

$$\phi = A \log(1/\delta) + A \log(X^2 + Y^2)^{1/2}.$$

As $X^2 + Y^2 \to 0$, the boundary layer solution (C.4) tends to

$$\phi \sim B + C \log(\pi(X^2 + Y^2)^{1/2}).$$

For these to match requires[4]

$$(C.5) \qquad A \log(1/\delta) = B + C \log \pi, \quad A = C.$$

Matching between the outer and boundary layer regions. Expanding the outer solution as $x \to 0$ gives

$$\phi \sim \phi(0) + x \frac{\partial \phi}{\partial x}(0) + \cdots.$$

Expanding the boundary layer solution (C.4) for large X gives

$$\phi \sim \pm C\pi X - C \log 2 + B \quad \text{as } X \to \pm\infty.$$

Matching these two expansions, recalling that $x = \epsilon X$, requires

$$(C.6) \qquad \left[\frac{\partial \phi}{\partial x}\right]_{x=0-}^{x=0+} = \frac{2\pi C}{\epsilon}, \quad \phi(0) = B - C \log 2.$$

Eliminating A, B and C between (C.5) and (C.6) gives the required effective boundary condition as

$$(C.7) \qquad \left[\frac{\partial \phi}{\partial x}\right]_{x=0-}^{x=0+} = \frac{2\pi}{\epsilon \log(1/(2\pi\delta))} \phi(0).$$

---

[4]Note that for δ small, B is much larger than C. We are simplifying the presentation by matching two orders of the expansion at the same time.

REFERENCES

[1] N. Anderson and A. M. Arthurs, Electrostatic screening, *Int. J. Electronics* 40 (1976), 289–292.

[2] S. Axler, P. Bourdon, and W. Ramey, *Harmonic Function Theory,* 2nd ed., Springer, 2001.

[3] P. Bövik, On the modelling of thin interface layers in elastic and acoustic scattering problems, *Quart. J. Mech. Appl. Math.,* 47 (1994), 17–42.

[4] K. F. Casey, Electromagnetic shielding behavior of wire-mesh screens, *IEEE Trans. Electromagnetic Compatibility,* 30 (1988), 298–306.

[5] D. Cioranescu and F. Murat, A strange term coming from nowhere, in Topics in the mathematical modelling of composite materials, *Progr. Nonlinear Differential Equations Appl.*, 31 (1997), 45–93.

[6] B. Delourme, *Modèles et asymptotiques des interface fines et périodiques en èletromagnètisme,* doctoral thesis, U. Pierre et Marie Curie, 2010.

[7] B. Delourme, H. Haddar, and P. Joly, Approximate models for wave propagation across thin periodic interfaces, *J. Math. Pures Appl.* 98 (2012), 28–71.

[8] B. Delourme, H. Haddar, and P. Joly, On the well-posedness, stability and accuracy of an asymptotic model for thin periodic interfaces in electromagnetic scattering problems, *Math. Models Methods Appl. Sci.* 23 (2013), 2433–2464.

[9] B. Engquist and J. C. Nédélec, Effective boundary conditions for acoustic and electromagnetic scattering in thin layers, Ecole Polytechnique–CMAP, 278 (1993).

[10] M. Faraday, *Experimental Researches in Electricity, v. 1,* reprinted from *Philosophical Transactions of* 1831–1838, Richard and John Edward Taylor, London, 1839 (paragraph 1174, p. 366); available at www.gutenberg.org/ebooks/14986.

[11] R. Feynman, R. B. Leighton, and M. Sands, *The Feynman Lectures on Physics, v. 2: Mainly Electromagnetism and Matter,* Addison-Wesley, 1964.

[12] J. Kevorkian and J. D. Cole, *Multiple Scale and Singular Perturbation Methods,* Springer, 1996.

[13] J. D. Kraus, *Electromagnetics,* 4th ed., McGraw-Hill, New York, 1992.

[14] H. Lamb, On the reflection and transmission of electric waves by a metallic grating, *Proc. Lond. Math. Soc.,* 29 (1898), 523–544.

[15] T. Larsen, A survey of the theory of wire grids, *IRE Trans. Microwave Theory and Techniques,* 10 (1962), 191–201.

[16] P. Martin, On acoustic and electric Faraday cages, *Proc. Roy. Soc. A* 470 (2014), 20140344.

[17] J. C. Maxwell, *A Treatise on Electricity and Magnetism*, v. 1, Clarendon Press, 1881 (secs. 203–205).

[18] R. Petit, Electromagnetic grating theories: limitations and successes, *Nouv. Rev. Optique,* 6 (1975), 129–135.

[19] J. Rauch and M. Taylor, Electrostatic screening, *J. Math. Phys.,* 16 (1975), 284–288.

[20] J. Rauch and M. Taylor, Potential and scattering theory on wildly perturbed domains, *J. Func. Anal.,* 18 (1975), 27–59.

[21] T. B. A. Senior and J. L. Volakis, Approximate boundary conditions in electromagnetics, *IEE Electromagnetic Waves Series*, 1995.

[22] L. N. Trefethen, Ten digit algorithms, Oxford technical report, http://people.maths.ox.ac.uk/trefethen/publication/PDF/2005_114.pdf.

[23] L. N. Trefethen and J. A. C. Weideman, The exponentially convergent trapezoidal rule, *SIAM Rev.* 56 (2014), 385–458.

[24] A. Zangwill, *Modern Electrodynamics,* Cambridge U. Press, 2013.